Doping-driven electronic and lattice dynamics in the phase-change material vanadium dioxide

Kannatassen Appavoo,[1,*] Joyeeta Nag,[2] Bin Wang,[2,3] Weidong Luo,[2,4,5] Gerd Duscher,[4,6] E. Andrew Payzant,[4] Matthew Y. Sfeir,[7] Sokrates T. Pantelides,[2,4,8] and Richard F. Haglund, Jr.[2,†]

[1]*Department of Physics, University of Alabama at Birmingham, Birmingham, Alabama 35294, USA*
[2]*Department of Physics and Astronomy, Vanderbilt University, Nashville, Tennessee 37235, USA*
[3]*School of Chemical, Biological, and Materials Engineering, University of Oklahoma, Norman, Oklahoma 73019, USA*
[4]*Center for Nanophase Materials Sciences, Oak Ridge National Laboratory, Oak Ridge, Tennessee 37831, USA*
[5]*Key Laboratory of Artificial Structures and Quantum Control, School of Physics and Astronomy, Shanghai Jiao Tong University, Shanghai 200240, China*
[6]*Department of Materials Science and Engineering, University of Tennessee, Knoxville, Tennessee 37996, USA*
[7]*Center for Functional Nanomaterials, Brookhaven National Laboratory, Upton, New York 11973, USA*
[8]*Department of Electrical Engineering and Computer Science, Vanderbilt University, Nashville, Tennessee 37235, USA*

(Received 15 February 2018; revised 23 December 2019; accepted 21 August 2020; published 23 September 2020)

Doping is generally understood as a strategy for including additional positive or negative charge carriers in a semiconductor, thereby tuning the Fermi level and changing its electronic properties in the equilibrium limit. However, because dopants also couple to all of the microscopic degrees of freedom in the host, they may also alter the nonequilibrium dynamical properties of the parent material, especially at large dopant concentrations. Here, we show how substitutional doping by tungsten at the 1 at. % level modifies the complex electronic and lattice dynamics of the phase-change material vanadium dioxide. Using femtosecond broadband spectroscopy, we compare dynamics in epitaxial thin films of pristine and tungsten-doped VO_2 over the broadest wavelength and temporal ranges yet reported. We demonstrate that coupling of tungsten atoms to the host lattice modifies the early electron-phonon dynamics on a femtosecond timescale, altering in a counterintuitive way the ps-to-ns optical signatures of the phase transition. Density functional theory correctly captures the enthalpy difference between pristine and W-doped VO_2 and shows how the dopant softens critical V-V phonon modes while introducing new phononic modes due to W-V bonds. While substitutional doping provides a powerful method to control the switching threshold and contrast of phase-change materials, determining how the dopant *dynamically* changes the broadband optical response is equally important for optoelectronics.

DOI: 10.1103/PhysRevB.102.115148

I. INTRODUCTION

The incorporation of dopant atoms into a crystalline or amorphous material is a ubiquitous technique in condensed-matter science that is also exploited in most solid-state device technologies [1,2]. Doping is typically a strategy for tuning the electronic structure of a material, thus modifying functional properties such as transport, space-charge depletion, or the dielectric function, either to elicit or to enhance certain phenomena or to satisfy specific requirements of a technology. For example, in reconfigurable technologies based on phase changes, such as optical data storage [3,4] and optoelectronics [5–7], doping a phase-change material (PCM) affects the electro-optical contrast between the initial and final states by initiating a change from metal to insulator or from a crystalline to an amorphous structure. In order for technologies based on PCMs to operate at THz speeds, it is equally important to understand how microscopic degrees of freedom that have been modified by dopant atoms respond dynamically to electronic or structural modification by an ultrafast light pulse. For example, in a PCM, the structural and electronic rearrangements play an important role in dictating key aspects of the transformation—including switching speed, energy cost, and dynamic modulation of the dielectric function. While the effect of doping on PCMs has been studied in thermal equilibrium for phase transitions induced by modulating heat, pressure, or electric fields, little is known about how doping alters the ultrafast electronic and structural response of doped PCMs [8–10].

Vanadium dioxide (VO_2) is a canonical PCM with competing crystalline phases that dictate its metallic and insulating properties [11–13] and appears to have significant applications in field-effect transistors [14] and ultrafast optoelectronics [10,15,16]. Vanadium dioxide exhibits a reversible solid-solid phase transformation that combines an insulator-to-metal transition (IMT) with a nearly simultaneous structural rearrangement from the monoclinic insulating (M1) phase to a rutile, tetragonal (R) form [17,18]. The discovery that the phase transition could be induced optically [19] has generated enormous interest in the potential of VO_2 thin films [10,20] and nanostructures [16] as all-optical switches.

Recent studies of the femtosecond photoinduced phase transition in VO_2 have focused on those processes with characteristic times less than 100 fs [10,15,21], effects of lattice

*Corresponding author: appavoo@uab.edu
†Corresponding author: richard.haglund@vanderbilt.edu

mismatch [22], and substrate thermal properties [23] during the transition. However, for VO_2 applications in photonics and electro-optics, it is also critical to understand whether or not doping can enable systematic tuning of the dynamics of light-induced IMT transition, such as switching-threshold fluence and relaxation times [20]. Yet remarkably, modifying the insulator-to-metal switching dynamics by doping VO_2 has not, to our knowledge, been attempted up to now. There is substantial evidence that the IMT can be induced by impulsive laser-driven hole doping on an ultrafast timescale [16,24], suggesting that the dynamics of the IMT may be controllable by changing the conduction-band population in the initial state. In particular, control of both the fluence threshold for switching and the relaxation dynamics from the metallic state would be desirable.

In this paper, we demonstrate that substitutional doping of tungsten at a level of approximately 1 at. % drastically modifies the dynamics of the photoinduced phase transition in VO_2, including both the coherent lattice response and charge-carrier dynamics. The fact that the doping occurs substitutionally, confirmed by atomic-resolution scanning-transmission electron microscopy, makes it possible to use density functional theory to calculate and interpret changes in the phonon spectrum and the effects of added carriers (here electrons) on the doped VO_2. Deploying broadband femtosecond spectroscopy, we show how the added electrons and microscopic deformations of the crystal lattice by the W dopants modifies the structural and electronic properties of VO_2 from femtosecond to nanosecond timescales. The added mass of the W-dopant atoms also modifies the electron-lattice coupling in the VO_2 host lattice, as seen in changes in the transient coherent phonon response of the system. The data presented here span the largest wavelength range and longest timescale of ultrafast measurements of the photoinduced phase transition in VO_2 yet measured, with or without doping. Moreover, the results suggest that doping can provide a general strategy for temporally tailoring the electro-optical contrast as well as the electron and phonon dynamics of PCMs.

II. FABRICATION AND STEADY-STATE CHARACTERIZATION

Epitaxial thin films of pristine and W-doped VO_2 were grown on c-cut sapphire (0001) using an established pulsed-laser deposition protocol [25]. The doped film was prepared using a 2 at. % W-doped V target to grow $W_{0.04}V_{0.96}O_2$ thin films. Rutherford backscattering, x-ray diffraction, and scanning electron microscopy (SEM) were employed to characterize both sets of samples and confirm that the tungsten dopants did not aggregate. In all studied samples, scanning electron micrographs displayed no substantial change in film texture. White-light transmission measurements showed that the W doping of VO_2 tunes the critical transition temperature downward [Figs. 1(a) vs 1(c)], here from $T_c = 70\,^{\circ}\mathrm{C}$ to $T_c = 48\,^{\circ}\mathrm{C}$, with changes both in the electronic and structural properties. The normalized white-light (WL) transmission also showed that W : VO_2 undergoes a more gradual phase transition than the pristine VO_2 when thermally cycled, exhibiting reduced optical contrast from about 42% in pristine VO_2 [Fig. 1(a)] to about 28% in W-doped VO_2 [Fig. 1(c)] relative to their respective low-temperature insulating states. Variable-temperature x-ray diffraction was employed to compare the *in situ* structural phase transition in both films, with 3D-isoline contours mapped onto two dimensions following the (010) monoclinic VO_2 family of planes that transform to the (100) tetragonal plane in the high-temperature state. The second- and fourth-order reflections of this (010) family of planes are tracked in the pristine [Fig. 1(b)] and W-doped [Fig. 1(d)] VO_2 films, respectively, as these have the highest intensity. In contrast to the sharp transition as pristine VO_2 evolves between the monoclinic and rutile structures, the W:VO_2 film shows a broader monoclinic peak that gradually and smoothly shifts to the tetragonal peak position when thermally cycled. This same contrast between abrupt versus gradual structural transitions is also evident in the signatures of the electronic transition (insulator to metal) in the WL-transmission hysteresis, and is consistent with observations in many experiments.

To determine unambiguously the location of the W ions, aberration-corrected atomic-number Z contrast scanning-transmission electron microscopy (STEM) was employed in combination with electron energy loss spectroscopy (EELS). Analysis of these data [Fig. 1(e)] reveals that the bright column (white arrow) is significantly more intense than the others and can be conclusively attributed to tungsten ions substituting for vanadium ions within the VO_2 lattice. This makes it possible to calculate the relative stability of the M1 and R phases both before and after doping using density functional theory, predicting the changes in critical temperature and enthalpy cost of the transition, as discussed in Sec. IV.

III. ULTRAFAST DYNAMICS IN PRISTINE VERSUS TUNGSTEN-DOPED VO_2

Figure 2 summarizes the effect of pump-laser fluence on the femtosecond dynamics of photon-induced phase transitions in pristine and W-doped VO_2 films in a transient-absorption experiment. Femtosecond transient absorption (TA) measurements were conducted using a commercial 1 kHz amplified Ti:sapphire laser system. Briefly, the pump pulse ($\lambda_{\mathrm{pump}} = 1100$ nm, pulse duration of about 50 fs) is the signal beam from a collinear optical parametric amplifier pumped by the 800 nm fundamental output of an amplified Ti:sapphire laser. The temporally synchronized probe pulse is a white-light supercontinuum generated by focusing the 800 nm light onto a sapphire crystal. The broadband probe yields rich insights into the complex, overlapping spectral signatures associated with the structural (phonon) and electronic dynamics [26,27] of VO_2, which change dramatically with pump fluence, particularly near switching thresholds.

Figure 2(a) shows the linear absorption of the metal and insulating phases (left axis) and optical-density contrast ($\Delta\mathrm{Ext}_{(\mathrm{M-I})}$) as a function of probe wavelength. For wavelengths shorter than 500 nm, the dielectric contrast between insulating and metallic states $\Delta\mathrm{Ext}_{(\mathrm{M-I})}$ is positive and small, indicating unambiguously the spectral range over which it is advantageous to compare the coherent phonon dynamics between pristine and W-doped VO_2 films [red stars in Figs. 2(a)–2(c)]. The coherent phonon dynamics results from displacive excitation of the A_1 "breathing modes" in the insulating-M1 state in VO_2 [28–30].

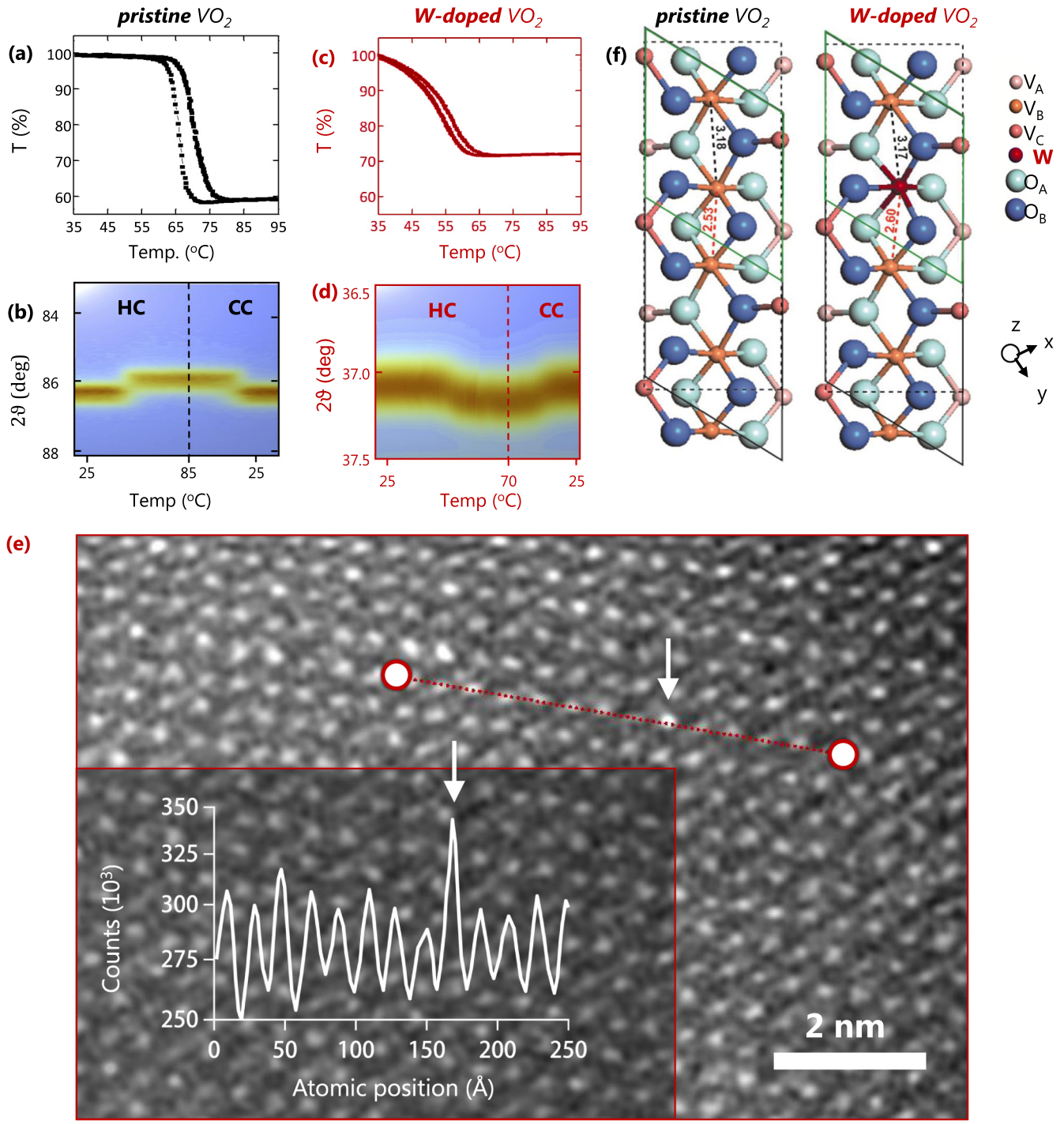

FIG. 1. Equilibrium electronic and structural properties of pristine and W-doped vanadium dioxide. (a), (c) White-light transmission measurements as a function of temperature and (b), (d) *in situ* x-ray diffraction rocking curves of the thermally induced insulator-to-metal transitions. "HC" and "CC" stand for heating and cooling cycle, respectively. The suppressed z axis in the projected 3D isoline contours is the diffraction intensity. (e) Atomic-number scanning-transmission electron micrograph (z-STEM) of the W-doped VO_2 sample, combined with electron energy loss spectroscopy (EELS). The inset is an electron beam intensity profile acquired by Fourier analysis of mass peaks along the row of atoms (measured in Å) marked by the red-colored dotted line. Evidence of substitutional doping allows for monoclinic structures of pristine and W-doped VO_2 to be calculated (f) using the density functional scheme described in the text. The W atom is represented in red here, with corresponding changes in the bond distances.

The near-IR pump pulse excites these A_1 Raman modes via displacive excitation of coherent phonons, with unusually large oscillation amplitudes that scale linearly with the fluence of the exciting pulse. When the metallic-R phase is generated from the insulating-M1 phase during ultrafast switching of VO_2, this transformation corresponds to a symmetry-breaking process with a vanishing coherent phonon dynamics. Increasing the pump fluence decreases the rise time for the metallic

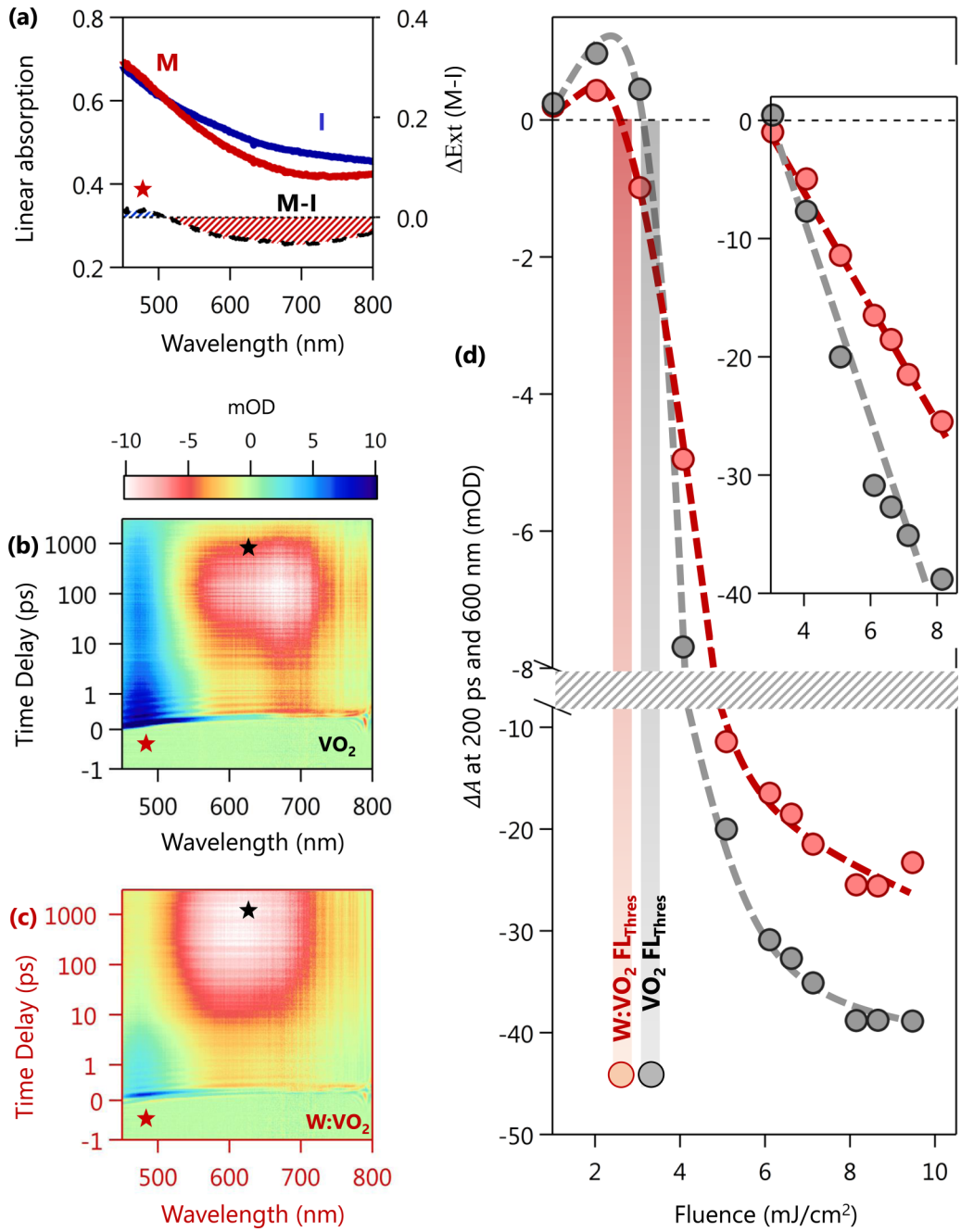

FIG. 2. Broadband Ultrafast Response of Pristine versus W-doped VO_2. (a) Linear extinction spectra of VO_2 in the insulating (blue) and metallic (red) state (left scale). The change in optical contrast (extinction) between the two states is also plotted in black dashed lines ($\Delta Ext_{(M-I)}$), right scale). Surface plots of visible-to-IR broadband transient response of (b) pristine and (c) W-doped VO_2 films excited at $\sim 3.5 mJ/cm^2$. The W-doped film shows completed switching behavior while the pristine VO_2 shows only a transient semiconductor response. For comparison purposes, the 2D color bar have been set to the same range for both samples. (d) Fluence-dependent measurements taken at 200 ps and averaged at ~600 nm for the pristine (grey) and W-doped VO_2 (red). Inset plots the same data on a linear scale to show that the slope ($|\Delta mOD/\Delta Fluence|$) is smaller for the W:$VO_2$ sample. Red and black stars highlight salient features of the ultrafast dynamics that are discussed in extensively in the main text.

phase to appear and, consequently, accelerates the decay of the coherent phonon dynamics. In fact, this coherent phonon signature has been successfully employed as a marker for monitoring the phase transition of VO_2 [10].

Figures 2(b) and 2(c) compare the two-dimensional time-resolved data taken for pristine and W-doped VO_2 samples excited by the same pump-laser fluence ($\sim 3.5 mJ/cm^2$)—corresponding to *below*-threshold excitation for pristine VO_2 [Fig. 2(b)] but *at-switching* threshold for $W:VO_2$ [Fig. 2(c)]—and reveal stark differences between doped and undoped material. The damped oscillatory signature of the coherent phonons is present for the pristine VO_2 even for

timescales greater than 5 ps (+ 5–10 mOD, red stars indicating the relevant spectral region). However, in the case of W-doped VO_2, the complex overlapping electronic signature is convoluted with the coherent phonon signature even for pump-probe time delays greater than 5 ps. Moreover, Fig. 2(c) provides an additional clue that $W:VO_2$ has been switched to its metallic state as the electronic response in the 550–750 nm range does not return to its ground state for times greater than 1000 ps (black star) [23,31]. The return of the original insulating-M1 phase takes place on a much longer timescale, a few tens to hundreds of nanoseconds [23]. For pristine VO_2 at the pump fluence of $\sim 3.5\,mJ/cm^2$, this electronic signature returns to its ground state within that same temporal window (black star), as is also the case for all lower pump fluences. Also, we note that for all pump fluences studied [Fig. 2(d)], W-doped VO_2 has a lower optical switching contrast, confirming that the change in conduction-band electron concentration has the same effect on the insulating state as "clamping" the temperature near the transition point [32,33].

Owing to the complex spectrotemporal signal—caused by the mixing of the signals from the coherent phonon dynamics (+mOD) and the electronic signature (-mOD)—we chose to compare our fluence-dependent measurement at 200 ps and at $\lambda = 600$ nm as an indicator of the phase transition. This is based on carefully analyzing all the 2D graphs for both the pristine and W-doped VO_2 samples and is summarized in Fig. 2(d). This point on the 2D surface plots allows a fair comparison between both broadband spectral response and fluence-dependent switching behaviors of both samples. However, this does not necessarily allow us to discriminate among mechanisms that could cause the switching of VO_2 to its metallic-R state; the switching could be caused either electronically via photohole doping or thermodynamically via carrier relaxation and subsequent carrier cooling that mediates the energy transfer to the lattice. Nevertheless, this figure reveals several key features of the $W:VO_2$ dynamics: (i) reduced optical contrast in the spectral range that corresponds to the coherent phonon vibrations for times less than 10 ps (lower positive values in the low-threshold fluence regime); (ii) a systematic and gradual reduction in optical contrast at every fluence; and (iii) a reduced switching threshold fluence $[F_{TH}(VO_2) - F_{TH}(W:VO_2) \sim 0.5\,mJ/cm^2]$ caused by the W dopant.

Figure 3 shows the differences in long-term dynamics when each sample is pumped at threshold, i.e., $\sim 3.5\,mJ/cm^2$ for $W:VO_2$ and $>4.0\,mJ/cm^2$ for VO_2. We extract the dynamics at three wavelengths to highlight their overall behavior. We can readily compare the response of these samples at threshold; we see for example that the coherent phonon signature is about three time stronger for the pristine VO_2 when compared to the $W:VO_2$, with the effect of coherent phonons being more pronounced at shorter wavelengths (here at $\lambda = 480$ nm). Moreover, for the case of the $W:VO_2$, the optical signatures of the coherent phonons exhibit overall a diminished amplitude and a qualitatively different oscillatory response compared to the VO_2 sample. This point is discussed further in Sec. IVB.

While optical techniques cannot definitively confirm changes in VO_2 structure across the phase transition, as ultrafast x-ray [13,34,35] and electron diffraction [36,37]

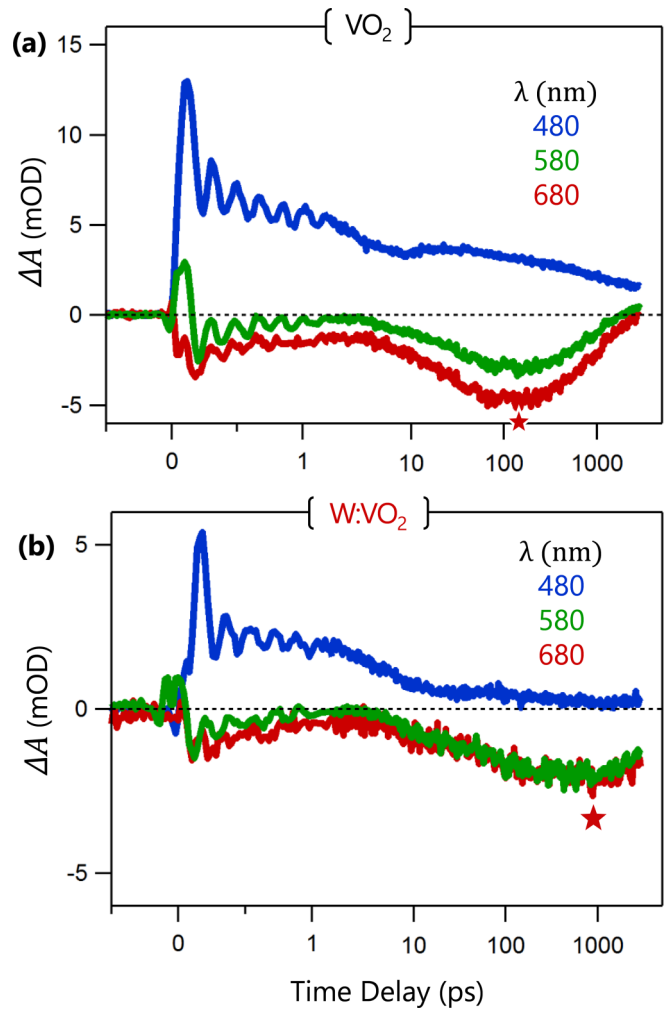

FIG. 3. Dynamics of pristine versus W-doped VO_2 at their respective switching thresholds. Transient absorption (TA) dynamic traces at various wavelengths ($\lambda = 480$, 580, and 680 nm) for (a) VO_2 at $3.5\,mJ/cm^2$ and (b) $W:VO_2$ at $4.0\,mJ/cm^2$ displaying the effect of changes in the coherent phonons on the optical signatures. The red star denotes the delay at which the samples have reached maximum change in optical contrast, corresponding to maximum R1 metallicities for the stated pump-laser fluence. Note the change in scale for the ordinate axis so as to display the coherent vibrations in the $W:VO_2$ sample.

experiments can, time-resolved optical measurements over very long timescales can lead to qualitatively correct insights because of the starkly different relaxation times of the metallic monoclinic and rutile phases. This is true even though, or in a way because, one is spatially averaging over many individual grains in the films, each grain switching probabilistically as the input pump laser energy thermalizes. The peak metallicity is larger in the undoped sample, consistent with the differing contrast ratios in Figs. 1(a) and 1(c). On the other hand, although $W:VO_2$ requires a lower optical fluence for switching, it reaches maximum metallicity at about 600 ps [red stars in Figs. 3(a) and 3(b)], which is delayed relative to pristine VO_2 (~150 ps). This is the case for all fluences above the switching threshold, suggesting that doping can control the temporal evolution

of VO_2 from the insulating monoclinic to the metallic, rutile state, accompanied by spectral changes in its broadband optical response. Importantly, our discussion of whether the samples have undergone the complete IMT is based on whether we observe electronic signatures (550–750 nm) that last for nanoseconds. We note also that our discussion revolves around the case when the sample reaches maximum metallicity, rather than defining a "unique" switching time for the various samples and excitation conditions.

Consistent with Booth *et al.* [38,39], and the data presented on thermal switching in the equilibrium regime [Figs. 1(a) and 1(b)], the principal effect of the W^{6+} dopant is to lower the energy required to switch the W-doped VO_2 film into the metallic state. The lattice distortion induced by the W-dopants extends over a few unit cells and modifies the energy requirement for switching. However, in contrast to the conclusion of Ref. [38] about a structurally driven IMT, Figs. 2(b) and 2(c) clearly show that the appearance of the structural phase transition to a metallic-R state is delayed. Therefore, the picosecond relaxation dynamics of carriers in the conduction band state and the slow growth of the metallic phase after 100 ps represent two distinct mechanisms. At the highest fluences studied, for both samples, band-gap collapse is nearly instantaneous and a subpicosecond insulator-to-metal transition occurs. This is consistent with recent demonstrations of instantaneous band-gap collapse that occurs within 100 fs after excitation to initiate a transition to the metallic rutile state, driven by hot carrier injection [16].

IV. THEORETICAL CALCULATIONS AND DISCUSSION

A. Effect of doping on enthalpy cost of phase transition

First-principles density functional theory (DFT) calculations were employed to evaluate the relative stability of the low-temperature monoclinic (M1) and high-temperature rutile (R) phases of VO_2 before and after W substitution, as depicted in Fig. 1(f). We used the Hohenberg-Kohn DFT [40,41] in the non-spin-polarized generalized-gradient approximation [42] plus Hubbard U (GGA+U) [43] approach and the projector augmented wave (PAW) method as implemented in VASP [44–46]. All calculations were performed with an energy cutoff of 500 eV. The Hubbard parameter and exchange interaction were $U = 4.0$ eV and $J = 0.7$ eV, respectively [16,47]. For pristine VO_2, the M1 unit cell contains four V atoms and eight O atoms, while the primitive unit cell of the R phase contains only two V atoms and four O atoms. For better convergence of the total energy difference between phases, a double unit cell, consistent in size and shape with the unit cell of the monoclinic phase, was used to calculate the rutile phase. An $8 \times 8 \times 8\,k$-point grid was generated using the Monkhorst-Pack scheme. The structures were relaxed so that residual forces on all atoms were smaller than 5×10^{-3} eV/Å. A supercell containing $WV_{31}O_{64}$ was used to compute the total energies of the W-doped monoclinic and rutile phases, corresponding to a W concentration of ~ 3 at. %, which is three times as large as the experimental doping, but it makes the calculations feasible.

The calculated M1 phase lattice parameters are $a = 5.68$ Å, $b = 4.61$ Å, $c = 5.45$ Å, with monoclinic angle $\alpha = 122.1^\circ$, in excellent agreement with experimental structure: $a = 5.7529$ Å, $b = 4.5263$ Å, $c = 5.3825$ Å, and $\alpha = 122.602^\circ$ [48]. For the rutile structure, the calculated relaxed structure corresponds to lattice parameters of $a = 4.64$ Å, $c = 2.80$ Å, in good agreement with experimental values of $a = 4.554$ Å, $c = 2.857$ Å. The calculated V-V distance in the rutile phase is 2.86 Å, while the short (long) V-V distances in the low-temperature M1 phase become 2.53 Å (3.18 Å), in good agreement with experiment. The total energy of the monoclinic phase is calculated to be lower than the rutile phase by 96.9 meV per VO_2 unit, consistent with the stability of the monoclinic phase at low temperature. For the calculated structure of the rutile phase, the VO_6 octahedron also has tetragonal symmetry. The four V-O bonds in the *a*-*b* plane have a length of 1.93 Å, while the two V-O bonds along the *c* direction have a length of 1.95 Å. For the calculated structure of the monoclinic phase, the VO_6 octahedron becomes distorted: The longest V-O bond becomes 2.07 Å, while the shortest V-O bond becomes 1.81 Å.

Following the definition of Baur [49] we can calculate the bond-length distortion index (DI) to quantify the distortion of the VO_6 octahedron: $\mathrm{DI} = \frac{1}{6}\sum_{i=1}^{6} |l_i - l_{\mathrm{av}}|/l_{\mathrm{av}}$, where l_i is the individual V-O bond length, and l_{av} is the average bond length. For the calculated rutile structure, DI = 0.002, indicating a small distortion of the VO_6 octahedron; while DI = 0.044 for the calculated monoclinic structure, indicating a larger distortion of the VO_6 octahedron. Following Robinson *et al.* [50], the variance of the octahedral bond angles in the VO_6 and WO_6 octahedra is defined as $\sigma^2 = \sum_{i=1}^{12} |\theta_i - 90^\circ|^2/11$, where θ_i is the individual angle between V-O (or W-O) bonds. For the calculated rutile structure, $\sigma^2 = 2.6\ \mathrm{deg}^2$, indicating very small distortion of the VO_6 octahedron, while $\sigma^2 = 39.9\ \mathrm{deg}^2$ for the calculated monoclinic structure, indicating large distortion of the VO_6 octahedron. For the W-doped monoclinic phase, both the WO_6 octahedron and its nearest-neighbor VO_6 octahedron are distorted less. We obtain $\sigma^2 = 33.3\ \mathrm{deg}^2$ for the WO_6 octahedron and $\sigma^2 = 28.0\ \mathrm{deg}^2$ for the neighboring VO_6 octahedron. The effects of W doping were calculated in a supercell containing 96 atoms with formula $WV_{31}O_{64}$, with atomic positions optimized for both M1 and R phases. The total energy of the monoclinic phase is lower than the rutile phase, consistent with the stability of even the W-doped M1 phase at low temperature. The total calculated energy difference is 74.4 meV per $W_{1/32}V_{31/32}O_2$ unit, which is smaller than that energy difference for undoped VO_2. Thus, W doping stabilizes the high-temperature rutile phase relative to the low-temperature monoclinic phase, consistent with the observed reduction of transition temperatures in W-doped VO_2 samples.

Assuming that the change of entropy between the monoclinic and rutile phases at the transition is the same for both pristine and W-doped VO_2, the phase-transition temperature $T_{C;1}$ of $W:VO_2$ can be estimated as $T_{C;1} = T_{C;0}(\Delta E_1/\Delta E_0)$, where $T_{C;0}$ is the transition temperature of pristine VO_2, and ΔE_0 and ΔE_1 are the total energy differences between the M1 and R phases in the VO_2 and $W:VO_2$, respectively. An estimated transition temperature of 261 K is obtained for the $WV_{31}O_{64}$ material using the calculated total energy differences and the experimental transition temperature of 340 K in pristine VO_2. The reduction of transition temperature in

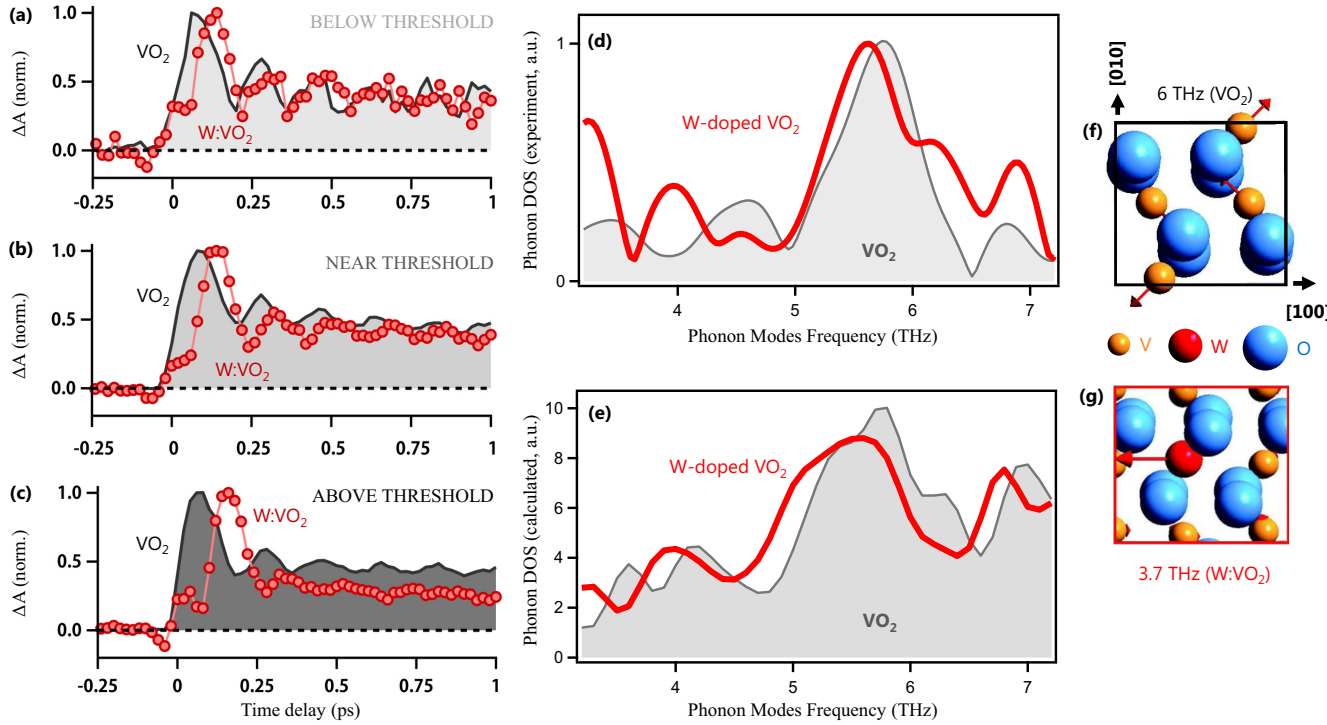

FIG. 4. Effect of W dopants on VO_2 coherent phonon dynamics. Normalized transient absorption (TA) data for only the first picosecond comparing VO_2 (gray) and W:VO_2 (red) at (a) below, (b) near, and (c) just above their respective switching thresholds. Note the systematic faster damping of the oscillation for the W-doped sample. (d) Experimental phonon spectra comparing pristine (gray) and tungsten-doped (red) VO_2 samples with lattice vibrations driven by below-threshold exciting pump pulse. Data were acquired by Fourier-transforming the kinetics data of Figs. 2(b) and 2(c) with spectral slices centered at 475 nm and with a 20 nm bandwidth. (e) Calculated phonon spectra at the Γ point using a finite displacement method comparing the VO_2 (gray) and W:VO_2 (red). The principal phonon vibrations for the V-V at 6 THz (for the VO_2 unit cell) and a representative 3.7 THz W-V mode in the 3.6–4.8 THz range (for the W:VO_2 unit cell) are shown in (f) and (g), respectively. The red atom represents the tungsten dopant.

W:VO_2 is equivalent to 25 K per 1% W-dopant atom, in excellent agreement with the experimentally observed reduction of 27 K per 1% W-dopant atom [51]. Consequently, the DFT calculations suggest that the differences in the structural phase transitions of pristine vs doped VO_2 films are associated with the structural distortion and additional charges introduced by the dopant ions. These changes in the energy cost of the transition are indeed reflected in the electronic signature of the phase change, that is, in the insulator-to-metal transition.

B. Effect of doping on coherent phonon dynamics

As suggested in Sec. III, the tungsten dopants have an appreciable effect on the lattice dynamics, on both the short and longer timescales (Fig. 3). To further quantify these effects in both samples, we extract the kinetic traces of the 2D time-resolved data at around 475 nm at key pump fluences [Figs. 4(a)–4(c)]. Figure 4(d) displays the experimentally obtained frequency domain signatures of the coherent phonons, acquired via Fourier transformation of the kinetic traces. The transformed data reveal that the W-dopant modifies the phonon spectrum by softening the VO_2 phonon modes. We observe phonon softening near 6 THz, a well-known signature of the phase transition in pristine VO_2 [10], as well as an additional phonon mode near 4 THz, near the Γ point. These lower-frequency V-W vibrational modes in the W-doped VO_2, when compared to the V-V dimer vibration at 6 THz in pristine VO_2 suggest that the presence of W may lower the energy required to trigger the phase change, resulting in the rather smooth transition observed in Fig. 2(c). As the fluence is increased to near-switching threshold and above, these phonon modes from both the pristine and W:VO_2 vanish, indicating the loss of the insulating state and the subsequent onset of metallization in the rutile crystalline structure.

To determine how the tungsten dopant modifies the phonon modes of the VO_2, vibrational frequencies were calculated using the zone-centered finite-difference method (Γ point only in the Brillouin zone), so that each ion is displaced in the direction of each Cartesian coordinate, as in density functional perturbation theory (DFPT). Using this finite-displacement method to calculate the lattice vibrations of this W-doped VO_2 system in a $WV_{107}O_{216}$ supercell, we find several zone-centered vibrations in the range 3.6–4.8 THz involving the motion of the W atom bonded to neighboring V atoms. In this approach, the Hessian matrix and the force constants were calculated using the VASP package [45]. The PBE-GGA exchange-correlation potential [52] was used, and the electron-core interactions were treated in the projector augmented wave (PAW) method [28,46]. All the calculations

were based on a supercell including 27 unit cells ($3 \times 3 \times 3$) of the monoclinic structure. For W-VO_2, one V atom is replaced by W, so that the W concentration is about 0.9%. The phonon density of states was calculated by manually counting the number of states within a 0.1 THz window and plotted as a function of frequency. The curves, as shown in Fig. 4(e), are smoothed using second-order least-squares regression to compare with the experimental data [Fig. 4(d)]. The calculations capture the phonon softening near 6 THz and the broadening and low-order modes near 4 THz. Figure 4(g) depicts a representative W-V mode in the 3.6–4.8 THz range for a W:VO_2 unit cell. The presence of lower-order modes is typically attributed to lattice vibrations that extend to multiple unit cells, as discussed by Gervais *et al.* [8]. Therefore, doping the VO_2 lattice with tungsten has the effect of modifying the phonon density of states at those lower phonon-mode frequencies.

V. CONCLUSION

We observe that both electronic and the structural phase transitions in VO_2 are strongly affected by substitutional doping of tungsten atoms, at a concentration appropriate to many phase-change applications. Ultrafast laser switching into the metallic state occurs at lower fluence in W-doped VO_2 films, with drastic time-dependent changes across the visible-to-NIR spectrum. Moreover, the difference in coherent response between pristine and W-doped VO_2 films suggests that bond softening due to both the higher electron concentration and greater inertial mass alters the carrier dynamics even during the first few picoseconds. The decreased transmission observed for the W-doped film at all fluences is attributable to the excess carriers in the conduction band, resulting also in a reduced energy required to switch the film. Another reason for this reduced transmission could be due to the dopant ions that generate localized regions of R-phase symmetry even in the insulating monoclinic VO_2 [21].

Doping with lighter elements, such as aluminum or magnesium [53,54], can, in principle, be used not only to control the switching threshold of a PCM, but also to change the optical contrast in the insulator-to-metal transmission and induce faster relaxation to the insulating state following ultrafast laser excitation. Dopants—either lighter or heavier than vanadium—can also be used to create lattice deformation in the form of strain, thus triggering the phase transition with varying switching threshold depending the nature of the strain (tensile or compressive) [55–57]. Localized introduction of dopants by ion implantation can be used to alter the optical properties of metamaterials and metasurfaces [58]. More rapid doping-induced dynamics would be appropriate for applications to silicon photonics, where optical and electrical switching of ring resonators using vanadium dioxide are already being explored [59,60].

In general, therefore, one can also expect that doping phase-change materials—with either excess electrons or holes—will continue to provide insights into phase-transition dynamics in strongly correlated materials, while simultaneously yielding many opportunities to control the properties of thin PCM films for specific applications in optoelectronics and photonics.

ACKNOWLEDGMENTS

Materials preparation and laser experiments were supported by the National Science Foundation (J.N. and R.F.H.: ECS-0801985; K.A.: OIA-1832898) and the Defense Threat Reduction Agency (K.A. and R.F.H.: HDTRA1-01-1-0047). Density functional theory (DFT) calculations were partly sponsored by the Department of Energy (Grant No. DE-FG02-09ER46554: B.W., W.L., and S.T.P.), by the National Science Foundation (Grant No. DMR-1207241: B.W., S.T.P.), and by the McMinn Endowment at Vanderbilt University (S.T.P.). This research used resources of the Center for Functional Nanomaterials, which is a US DOE Office of Science Facility, at Brookhaven National Laboratory under Contract No. DE-SC0012704. Computations were performed at the National Energy Research Scientific Computing Center. Portions of this work were performed at the Vanderbilt Institute of Nanoscale Science and Engineering, using facilities renovated under NSF ARI-R2 DMR-0963361. The high-temperature XRD work was conducted at the Center for Nanophase Materials Sciences, which is a DOE Office of Science User Facility. We thank Prof. Simon Wall and Prof. Raanan Tobey for helpful discussions.

[1] N. W. Ashcroft and N. D. Mermin, *Solid State Physics* (Brooks Cole, 1976).

[2] M. D. Archer and A. J. Nozik, *Nanostructured and Photoelectrochemical Systems for Solar Photon Conversion* (World Scientific, 2003).

[3] M. Wuttig and N. Yamada, Phase-change materials for rewriteable data storage, Nat. Mater. **6**, 824 (2007).

[4] S. Raoux and M. Wuttig (Eds.), *Phase Change Materials: Science and Applications* (Springer, Boston, MA, 2009).

[5] Q. Xu, B. Schmidt, S. Pradhan, and M. Lipson, Micrometre-scale silicon electro-optic modulator, Nature (London) **435**, 325 (2005).

[6] J. Y. Ou, E. Plum, L. Jiang, and N. I. Zheludev, Reconfigurable photonic metamaterials, Nano Lett. **11**, 2142 (2011).

[7] C. Ríos, M. Stegmaier, P. Hosseini, D. Wang, T. Scherer, C. D. Wright, H. Bhaskaran, and W. H. P. Pernice, Integrated all-photonic non-volatile multi-level memory, Nat. Photonics **9**, 725 (2015).

[8] F. Gervais and W. Kress, Lattice dynamics of oxides with rutile structure and instabilities at the metal-semiconductor phase transitions of NbO_2 and VO_2, Phys. Rev. B **31**, 4809 (1985).

[9] H. Wei and J. Huang, Halide lead perovskites for ionizing radiation detection, Nat. Commun. **10**, 1066 (2019).

[10] S. Wall, D. Wegkamp, L. Foglia, K. Appavoo, J. Nag, R. F. Haglund, Jr., J. Staehler, and M. Wolf, Ultrafast changes in lattice symmetry probed by coherent phonons, Nat. Commun. **3**, 721 (2012).

[11] M. M. Qazilbash, M. Brehm, B.-G. Chae, P. C. Ho, G. O. Andreev, B.-J. Kim, S. J. Yun, A. V. Balatsky, M. B. Maple, F. Keilmann, H.-T. Kim, and D. N. Basov, Mott transition in VO_2 revealed by infrared spectroscopy and nano-imaging, Science **318**, 1750 (2007).

[12] D. N. Basov, R. D. Averitt, D. van der Marel, M. Dressel, and K. Haule, Electrodynamics of correlated electron materials, Rev. Mod. Phys. **83**, 471 (2011).

[13] S. Wall, S. Yang, L. Vidas, M. Chollet, J. M. Glownia, M. Kozina, T. Katayama, T. Henighan, M. Jiang, T. A. Miller, D. A. Reis, L. A. Boatner, O. Delaire, and M. Trigo, Ultrafast disordering of vanadium dimers in photoexcited VO_2, Science **362**, 572 (2018).

[14] Z. Yang, C. Ko, and S. Ramanathan, Oxide electronics utilizing ultrafast metal-insulator transitions, Ann. Rev. Mater. Res. **41**, 337 (2011).

[15] D. Wegkamp, M. Herzog, L. Xian, M. Gatti, P. Cudazzo, C. L. McGahan, R. E. Marvel, R. F. Haglund, A. Rubio, M. Wolf, and J. Stähler, Instantaneous Band Gap Collapse in Photoexcited Monoclinic VO_2 due to Photocarrier Doping, Phys. Rev. Lett. **113**, 216401 (2014).

[16] K. Appavoo, B. Wang, N. F. Brady, M. Seo, J. Nag, R. P. Prasankumar, D. J. Hilton, S. T. Pantelides, and R. F. Haglund, Ultrafast phase transition via catastrophic phonon collapse driven by plasmonic hot-electron injection, Nano Lett. **14**, 1127 (2014).

[17] H. W. Verleur, A. S. Barker, and C. N. Berglund, Optical properties of VO_2 between 0.25 and 5 eV, Phys. Rev. **172**, 788 (1968).

[18] C. N. Berglund and H. J. Guggenhe, Electronic properties of VO_2 near semiconductor-metal transition, Phys. Rev. **185**, 1022 (1969).

[19] W. R. Roach and I. Balberg, Optical induction and detection of fast phase transition in VO_2, Solid State Commun. **9**, 551 (1971).

[20] A. Cavalleri, C. Toth, C. W. Siders, J. A. Squier, F. Raksi, P. Forget, and J. C. Kieffer, Femtosecond Structural Dynamics in VO_2 during an Ultrafast Solid-Solid Phase Transition, Phys. Rev. Lett. **87**, 237401 (2001).

[21] M. F. Jager, C. Ott, P. M. Kraus, C. J. Kaplan, W. Pouse, R. E. Marvel, R. F. Haglund, D. M. Neumark, and S. R. Leone, Tracking the insulator-to-metal phase transition in VO_2 with few-femtosecond extreme UV transient absorption spectroscopy, Proc. Natl. Acad. Sci. USA **114**, 9558 (2017).

[22] S. Lysenko, A. Rua, V. Vikhnin, F. Fernandez, and H. Liu, Insulator-to-metal phase transition and recovery processes in VO_2 thin films after femtosecond laser excitation, Phys. Rev. B **76**, 035104 (2007).

[23] N. F. Brady, K. Appavoo, M. Seo, J. Nag, R. P. Prasankumar, R. F. Haglund, Jr., and D. J. Hilton, Heterogeneous nucleation and growth dynamics in the light-induced phase transition in vanadium dioxide, J. Phys.: Condens. Matter **28**, 125603 (2016).

[24] C. Kubler, H. Ehrke, R. Huber, R. Lopez, A. Halabica, R. F. Haglund, Jr., and A. Leitenstorfer, Coherent Structural Dynamics and Electronic Correlations during an Ultrafast Insulator-to-Metal Phase Transition in VO_2, Phys. Rev. Lett. **99**, 116401 (2007).

[25] J. Nag, E. A. Payzant, K. L. More, and R. F. Haglund, Jr., Enhanced performance of room-temperature-grown epitaxial thin films of vanadium dioxide, Appl. Phys. Lett. **98**, 251916 (2011).

[26] M. Rini, A. Cavalleri, R. W. Schoenlein, R. Lopez, L. C. Feldman, R. F. Haglund, L. A. Boatner, and T. E. Haynes, Photoinduced phase transition in VO_2 nanocrystals: Ultrafast control of surface-plasmon resonance, Opt. Lett. **30**, 558 (2005).

[27] K. Appavoo, D. Y. Lei, Y. Sonnefraud, B. Wang, S. T. Pantelides, S. A. Maier, and R. F. Haglund, Role of defects in the phase transition of VO_2 nanoparticles probed by plasmon resonance spectroscopy, Nano Lett. **12**, 780 (2012).

[28] H. J. Zeiger, J. Vidal, T. K. Cheng, E. P. Ippen, G. Dresselhaus, and M. S. Dresselhaus, Theory for displacive excitation of coherent phonons, Phys. Rev. B **45**, 768 (1992).

[29] G. L. Cohen, J. Garcia, V. Purdie-Vaughns, N. Apfel, and P. Brzustoski, Recursive processes in self-affirmation: intervening to close the minority achievement gap, Science **324**, 400 (2009).

[30] T. K. Cheng, L. H. Acioli, J. Vidal, H. J. Zeiger, G. Dresselhaus, M. S. Dresselhaus, and E. P. Ippen, Modulation of a semicondutor-to-semimetal transition at 7 THz via coherent lattice vibrations, Appl. Phys. Lett. **62**, 1901 (1993).

[31] M. C. Newton, M. Sao, Y. Fujisawa, R. Onitsuka, T. Kawaguchi, K. Tokuda, T. Sato, T. Togashi, M. Yabashi, T. Ishikawa, T. Ichitsubo, E. Matsubara, Y. Tanaka, and Y. Nishino, Time-resolved coherent diffraction of ultrafast structural dynamics in a single nanowire, Nano Lett. **14**, 2413 (2014).

[32] D. J. Hilton, R. P. Prasankumar, S. Fourmaux, A. Cavalleri, D. Brassard, M. A. El Khakani, J. C. Kieffer, A. J. Taylor, and R. D. Averitt, Enhanced Photosusceptibility near T_c for the Light-Induced Insulator-to-Metal Phase Transition in Vanadium Dioxide, Phys. Rev. Lett. **99**, 226401 (2007).

[33] A. Pashkin, C. Kubler, H. Ehrke, R. Lopez, A. Halabica, R. F. Haglund, R. Huber, and A. Leitenstorfer, Ultrafast insulator-metal phase transition in VO_2 studied by multiterahertz spectroscopy, Phys. Rev. B **83**, 195120 (2011).

[34] X. Tan, T. Yao, R. Long, Z. Sun, Y. Feng, H. Cheng, X. Yuan, W. Zhang, Q. Liu, C. Wu, Y. Xie, and S. Wei, Unraveling metal-insulator transition mechanism of VO_2 triggered by tungsten doping, Sci. Rep. **2**, 466 (2012).

[35] L. Vidas, D. Schick, E. Martínez, D. Perez-Salinas, S. Cichy, S. Batlle-Porro, K. A. Hallman, R. F. Haglund, Jr., and S. Wall, Does VO_2 Host a Transient Monoclinic Metallic Phase? Phys. Rev. X **10**, 031047 (2020).

[36] M. R. Otto, L. P. René de Cotret, D. A. Valverde-Chavez, K. L. Tiwari, N. Émond, M. Chaker, D. G. Cooke, and B. J. Siwick, How optical excitation controls the structure and properties of vanadium dioxide, Proc. Natl. Acad. Sci. USA **116**, 450 (2019).

[37] Z. Tao, T.-R. T. Han, S. D. Mahanti, P. M. Duxbury, F. Yuan, C.-Y. Ruan, K. Wang, and J. Wu, Decoupling of Structural and Electronic Phase Transitions in VO_2, Phys. Rev. Lett. **109**, 166406 (2012).

[38] J. M. Booth and P. S. Casey, Anisotropic Structure Deformation in the VO_2 Metal-Insulator Transition, Phys. Rev. Lett. **103**, 086402 (2009).

[39] J. M. Booth, D. W. Drumm, P. S. Casey, J. S. Smith, and S. P. Russo, Electronic structure of tungsten-doped vanadium dioxide, arXiv:1507.00105.

[40] P. Hohenberg and W. Kohn, Inhomogeneous Electron Gas, Phys. Rev. **136**, B864 (1964).

[41] W. Kohn and L. J. Sham, Self-Consistent Equations Including Exchange and Correlation Effects, Phys. Rev. **140**, A1133 (1965).

[42] J. P. Perdew, K. Burke, and Y. Wang, Generalized gradient approximation for the exchange-correlation hole of a many-electron system, Phys. Rev. B **54**, 16533 (1996).

[43] V. I. Anisimov, J. Zaanen, and O. K. Andersen, Band theory and Mott insulators: Hubbard U instead of Stoner I, Phys. Rev. B **44**, 943 (1991).

[44] P. E. Blochl, Projector augmented-wave method, Phys. Rev. B **50**, 17953 (1994).

[45] G. Kresse and J. Furthmuller, Efficient iterative schemes for *ab initio* total-energy calculations using a plane-wave basis set, Phys. Rev. B **54**, 11169 (1996).

[46] G. Kresse and D. Joubert, From ultrasoft pseudopotentials to the projector augmented-wave method, Phys. Rev. B **59**, 1758 (1999).

[47] S. Biermann, A. Poteryaev, A. I. Lichtenstein, and A. Georges, Dynamical Singlets and Correlation-Assisted Peierls Transition in VO_2, Phys. Rev. Lett. **94**, 026404 (2005).

[48] K. D. Rogers, An x-ray diffraction study of semiconductor and metallic vanadium dioxide, Powder Diffr. **8**, 240 (1993).

[49] W. Baur, The geometry of polyhedral distortions: Predictive relationships for the phosphate group, Acta Crystallogr., Sect. B **30**, 1195 (1974).

[50] K. Robinson, G. V. Gibbs, and P. H Ribbe, Quadratic elongation: A quantitative measure of distortion in coordination polyhedra, Science **172**, 567 (1971).

[51] J. C. Rakotoniaina, R. Mokrani-Tamellin, J. R. Gavarri, G. Vacquier, A. Casalot, and G. Calvarin, The thermochromic vanadium dioxide: I. Role of stresses and substitution on switching properties, J. Solid State Chem. **103**, 81 (1993).

[52] J. P. Perdew, K. Burke, and M. Ernzerhof, Generalized Gradient Approximation Made Simple, Phys. Rev. Lett. **77**, 3865 (1996).

[53] E. Strelcov, A. Tselev, I. Ivanov, J. D. Budai, J. Zhang, J. Z. Tischler, I. Kravchenko, S. V. Kalinin, and A. Kolmakov, Doping-based stabilization of the M2 phase in free-standing VO_2 nanostructures at room temperature, Nano Lett. **12**, 6198 (2012).

[54] C. G. Granqvist, I. B. Pehlivan, Y. X. Ji, S. Y. Li, and G. A. Niklasson, Electrochromics and thermochromics for energy efficient fenestration: Functionalities based on nanoparticles of In_2O_3: Sn and VO_2, Thin Solid Films **559**, 2 (2014).

[55] K. Sokolowski-Tinten, C. Blome, J. Blums, A. Cavalleri, C. Dietrich, A. Tarasevitch, I. Uschmann, E. Forster, M. Kammler, M. Horn-von-Hoegen, and D. von der Linde, Femtosecond x-ray measurement of coherent lattice vibrations near the Lindemann stability limit, Nature (London) **422**, 287 (2003).

[56] M. Forst, A. D. Caviglia, R. Scherwitzl, R. Mankowsky, P. Zubko, V. Khanna, H. Bromberger, S. B. Wilkins, Y. D. Chuang, W. S. Lee, W. F. Schlotter, J. J. Turner, G. L. Dakovski, M. P. Minitti, J. Robinson, S. R. Clark, D. Jaksch, J. M. Triscone, J. P. Hill, S. S. Dhesi, and A. Cavalleri, Spatially resolved ultrafast magnetic dynamics initiated at a complex oxide heterointerface, Nat. Mater. **14**, 883 (2015).

[57] M. Porer, U. Leierseder, J. M. Ménard, H. Dachraoui, L. Mouchliadis, I. E. Perakis, U. Heinzmann, J. Demsar, K. Rossnagel, and R. Huber, Non-thermal separation of electronic and structural orders in a persisting charge density wave, Nat. Mater. **13**, 857 (2014).

[58] J. Rensberg, S. Zhang, Y. Zhou, A. S. McLeod, C. Schwarz, M. Goldflam, M. K. Liu, J. Kerbusch, R. Nawrodt, S. Ramanathan, D. N. Basov, F. Capasso, C. Ronning, and M. A. Kats, Active optical metasurfaces based on defect-engineered phase-transition materials, Nano Lett. **16**, 1050 (2016).

[59] J. D. Ryckman, K. A. Hallman, R. E. Marvel, R. F. Haglund, and S. M. Weiss, Ultra-compact silicon photonic devices reconfigured by an optically induced semiconductor-to-metal transition, Opt. Express **21**, 10753 (2013).

[60] P. Markov, R. E. Marvel, H. J. Conley, K. J. Miller, R. F. Haglund, Jr., and S. M. Weiss, Optically monitored electrical switching in VO_2, ACS Photonics **2**, 1175 (2015).